Nutrient dynamics in the winter thermohaline frontal zone of the northern shelf region of the South China Sea

Su Mei Liu,[1] Xinyu Guo,[2] Qi Chen,[3] Jing Zhang,[1,4] Yan Feng Bi,[1] Xin Luo,[1] and Jian Bing Li[1]

Received 30 October 2009; revised 23 May 2010; accepted 29 June 2010; published 23 November 2010.

[1] As the first attempt to estimate the nutrient transport across the winter thermohaline frontal zone on the northern shelf of the South China Sea, the nutrient dynamics around the front and the effects of cross-frontal water exchange on nutrient transport were investigated using wintertime field observations. Both water temperature and salinity increased from coastal to oceanic waters, showing the presence of a thermohaline front. The concentrations of dissolved inorganic nutrients decreased oceanward, especially across the thermohaline front, while those of dissolved organic nutrients (i.e., dissolved organic nitrogen (DON) and dissolved organic phosphorus) showed patchy distributions. Ammonium was the major constituent of dissolved inorganic nitrogen, and DON was the main component of total dissolved nitrogen. Molar ratios of PO_4^{3-}/total dissolved phosphorus decreased from coastal to oceanic waters, indicating that PO_4^{3-} was rapidly removed and/or consumed from the water column and that organic matter degradation increased offshore, replenishing PO_4^{3-}. Molar ratios of $NO_3^-/(NH_4^+ + DON)$ were 0.01–0.6, indicating dominance of regenerated nitrogen. Surface water convergence and bottom water divergence were identified in the across-shore velocity field, and the calculated across-shore nutrient fluxes suggest that the presence of the winter thermohaline front promotes the offshore transport of nutrients from coastal waters. The transport path begins with convergence of surface coastal waters toward the front, followed by the sinking in the frontal region and the oceanward movement through the bottom layer of the front offshore side. With an assumption of 500 km as the length of thermohaline front on the northern shelf of the South China Sea, the calculated offshore fluxes of nutrients across the entire front are larger than those from the Zhujiang (Pearl River) and the Changjiang (Yangtze River).

Citation: Liu, S. M., X. Guo, Q. Chen, J. Zhang, Y. F. Bi, X. Luo, and J. B. Li (2010), Nutrient dynamics in the winter thermohaline frontal zone of the northern shelf region of the South China Sea, *J. Geophys. Res.*, *115*, C11020, doi:10.1029/2009JC005951.

1. Introduction

[2] Fronts are often observed in the ocean, but the characteristics of one front can be completely different from the others. *Yanagi* [1987] classified the fronts into coastal water fronts, shelf fronts, and open ocean fronts and summarized that there are four types of fronts in coastal waters. Estuarine fronts are located near river mouth or along with river plume, thermal effluent fronts are close to power plants, thermohaline fronts are formed in transition zones between cold coastal waters and warm oceanic waters in winter, and tidal fronts are formed in transition zones between vertical mixed waters attributed to tidal stirring and stratified waters in summer. If we consider a region far from river mouth and a power plant, only thermohaline fronts are expected in coastal waters in winter.

[3] The formation of thermohaline fronts depends on wintertime atmospheric cooling and salinity difference between the coastal area and the offshore area. Because of atmospheric cooling, the waters are colder in the shallow coastal area than in the deep offshore area. River discharge keeps the salinity lower in the coastal area than in the deep offshore area. If the differences in water temperature and salinity between the coastal area and the offshore area allow the presence of a surface convergence zone, thermohaline fronts with strong horizontal temperature and salinity gradients are generated [*Endoh*, 1977; *Akitomo et al.*, 1990]. The density difference across the thermohaline fronts is

[1]Key Laboratory of Marine Chemistry Theory and Technology, Ministry of Education, Ocean University of China, Qingdao, China.
[2]Center for Marine Environmental Studies, Ehime University, Matsuyama, Japan.
[3]Laboratory of Ocean Dynamic Processes and Satellite Oceanography, Second Institute of Oceanography, State Oceanic Administration, Hangzhou, China.
[4]State Key Laboratory of Estuarine and Coastal Research, East China Normal University, Shanghai, China.

Copyright 2010 by the American Geophysical Union.
0148-0227/10/2009JC005951

small, but a weak density peak caused by the cabbeling effect can be found in the frontal region [*Endoh*, 1977; *Akitomo et al.*, 1990]. These fronts have been identified in many western Pacific coastal areas such as the Kii Channel [*Yoshioka*, 1971], Tokyo Bay [*Yanagi and Sanuki*, 1991], and Ise Bay [*Yanagi et al.*, 1997] based on hydrographic observations. Studies using satellite data and numerical models also suggested the presence of thermohaline fronts in the South China Sea (SCS) in winter [*Wang et al.*, 2001; *Chu and Wang*, 2003].

[4] The SCS is an epi-continental marginal sea of the western Pacific Ocean, with a surface area of 350×10^4 km^2 and an average water depth of 1212 m. The SCS is a Mediterranean-type basin dominated by monsoon circulation, which travels northeasterly from October to April and southwesterly from May to September. The northern part of the SCS has a wide shallow shelf, and several rivers empty into this region, including the Zhujiang (Pearl River).

[5] The coastal zone in the northern SCS is China's most populated area and has the most developed economy in China. Consequently, eutrophication is a serious problem, and harmful algal blooms occur frequently [*Song et al.*, 2004; *Yin and Harrison*, 2007]. On the other hand, the basin-wide SCS is devoid of nutrients in the surface layer. The concentration of nutrients increases with depth [*Chen et al.*, 2001], and the deepwater maximum of nutrients is shallow and smooth because of its rapid ventilation and short flushing time relative to the open ocean [*Zhang and Su*, 2006].

[6] The primary production in the SCS is higher in winter than in summer [*Liu et al.*, 2002; *Ning et al.*, 2004; *Lee Chen*, 2005; *Chen et al.*, 2006; *Lee Chen and Chen*, 2006]. This seasonal variation of phytoplankton depends closely on the wind surface mixing that is stronger in winter than in summer and therefore brings more nutrients to surface layer in winter. In addition, the material transport across the thermohaline front is also a possible mechanism for the nutrient sources in the SCS in winter because water transport across fronts plays a significant role in nondiffusive biogeochemical material transport processes [*Read et al.*, 2000; *Naveiragarabato et al.*, 2002; *Li et al.*, 2003], which influence the distributions of nutrients, phytoplankton, and zooplankton and hence affect the stability of the ecosystem [*Kachel et al.*, 2002].

[7] Although a thermal front in the SCS has been identified with wintertime satellite data [*Wang et al.*, 2001], there has not been a field report on salinity and nutrient distributions around the front yet. Furthermore, nutrient transport in relation to the front in the SCS is also unknown. On the other hand, quite different picoplankton group dynamics have been observed across the thermohaline front in the northern SCS shelf [*Pan et al.*, 2005]. Therefore, it is necessary to clarify nutrient distributions around the thermohaline front and to determine the role of the front on nutrient transport.

2. Materials and Methods

[8] Field observations were performed on the northern SCS shelf from 27 January to 6 February 2004. Hydrographic surveys and water sampling occurred at stations along sections A, C, F, and G (Figure 1). Only sections A and G are presented here to examine the influence of the thermohaline front on nutrient transports by comparing the nutrient fluxes in the presence (such as section A) and absence (such as section G) of the thermohaline front. Anchor stations were maintained at stations A3 and A6 for over 25 h, during which measurements were performed every 3 h for chemical parameters and each hour for hydrographical parameters and current profiles.

[9] Vertical temperature, salinity, and current profiles were measured with a SBE25-CTD and a Lowered Acoustic Doppler Current Profiler (LADCP; Teledyne RDI 1200 kHz). The current data measured by LADCP at each station were processed with the Teledyne RDI standard software. The current data are available from 3 to 30 m depth with a vertical interval of 1 m. Assuming that the current did not change from sea surface to 3 m depth and was zero at sea bottom, we extrapolated the current data to the layer shallower than 3 m and the layer deeper than 30 m depth.

[10] Discrete water samples were collected in 10 L Niskin bottles attached to a conductivity-temperature-depth (CTD) rosette, and sampling depths were determined by assessing hydrographic parameters. After water collection, samples were immediately filtered through precleaned 0.45 μm pore cellulose acetate filters, and the filtrates were poisoned with saturated $HgCl_2$.

[11] Nutrient concentrations (NO_3^-, NO_2^-, NH_4^+, PO_4^{3-}, and $Si(OH)_4$) were quantified using an autoanalyzer (Skalar SAN^{plus}) [*Liu et al.*, 2005]. The analytical precision of NO_2^-, NO_3^-, NH_4^+, PO_4^{3-}, and $Si(OH)_4$ was 0.01, 0.06, 0.09, 0.03, and 0.15 μM, respectively. The dissolved inorganic nitrogen (DIN) concentration is the sum of NO_3^-, NO_2^-, and NH_4^+. Total dissolved nitrogen (TDN) and total dissolved phosphorus (TDP) were treated with boracic acid-persulfate oxidation solution ($K_2S_2O_8$ and H_3BO_3 in NaOH solution) in an autoclave and hydrolyzed at 120°C for 30 min. Then, TDN and TDP were decomposed to NO_3^- and PO_4^{3-}, respectively, and measured using an autoanalyzer [*Grasshoff et al.*, 1999]. The analytical precision of TDN and TDP was 0.68 and 0.02 μM, respectively. Dissolved organic nitrogen (DON) and dissolved organic phosphorus (DOP) concentrations were estimated as the difference between TDN and DIN or TDP and PO_4^{3-}, respectively. Duplicate samples were run, and the precision for DON and DOP was 5% and 15%, respectively.

3. Results

3.1. Hydrographic Characteristics

[12] At section A, both water temperature and salinity increased from coastal (<15.5°C and <33.45 salinity) to oceanic waters (>20.5°C and >34.6 salinity) (Figure 2). A strong thermohaline front was observed between stations A4 and A5, with temperature and salinity gradients of 0.75°C km^{-1} and 0.25 km^{-1}, respectively. On the front onshore side, inverse temperature layers (17°C) were found at the bottom layer of station A3; on the front offshore side, low-salinity layers (<34.3) were found along the bottom layer. Above the inverse temperature and low-salinity layers, the water column was vertically well mixed. The water density in the surface layer was highest at the front region and decreased toward its offshore and onshore sides. In the vertical, the increase in water density from the surface

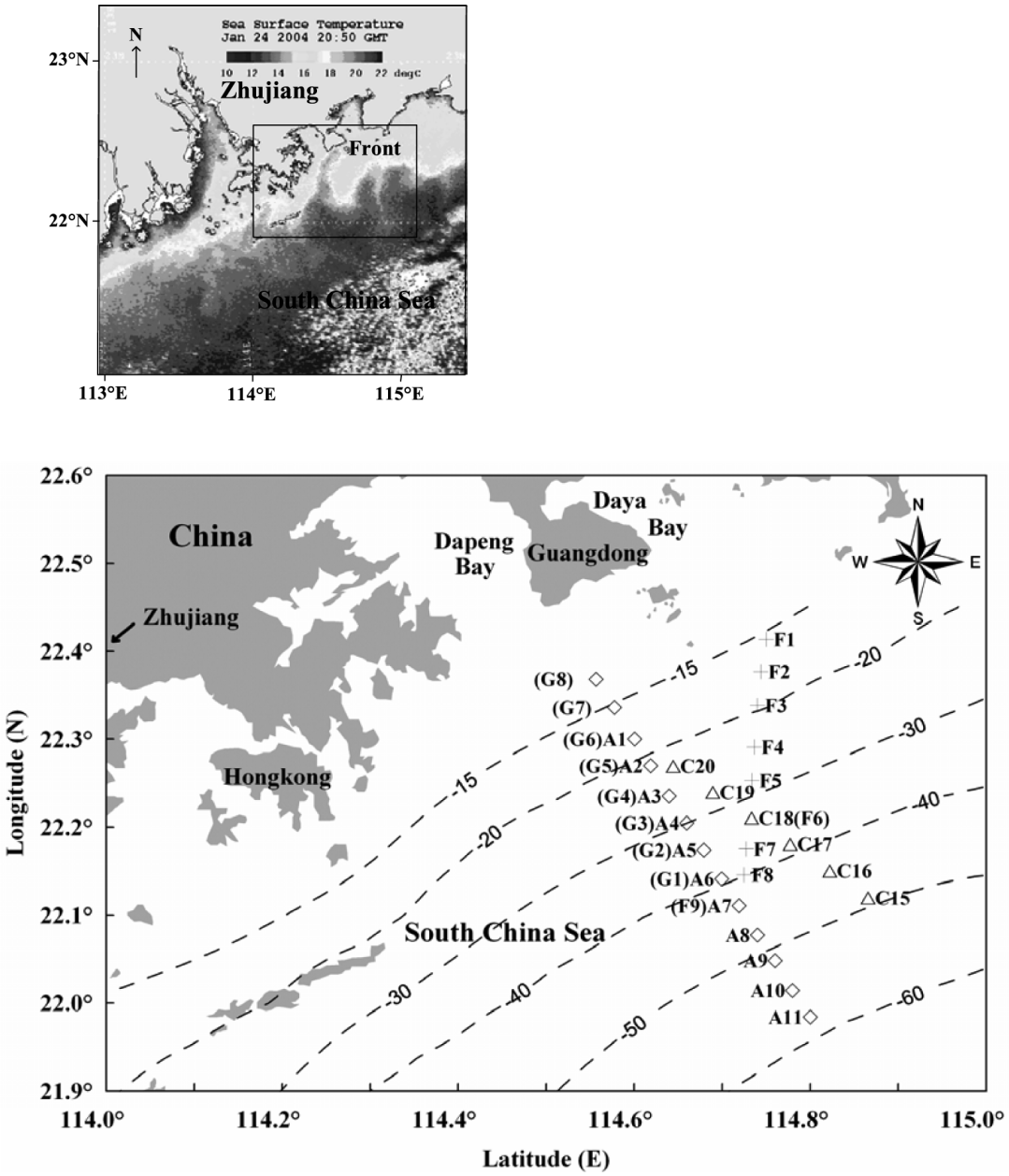

Figure 1. (top) Advanced very high resolution radiometer infrared image of the northern part of the South China Sea, taken on 24 January 2004 (courtesy of J.-C. Chen, Center for Astrodynamics Research, Hong Kong University of Science and Technology). (bottom) Map of stations along legs A and C (i.e., stations A1–A11 and C16–C20) and legs F and G (i.e., stations F1–F9 and G1–G8). Only sections A and G are presented in this study to examine the influence of the thermohaline front on nutrient transports by comparing the nutrient fluxes in the presence (such as section A) and absence (such as section G) of the thermohaline front.

layer toward the bottom layer occurred at both the front region and its two sides. If we consider the convergence of two water masses with different water temperature and salinity but similar density (oceanic water with high water temperature and high salinity, coastal water with low water temperature and low salinity) toward the front, the spatial structure of density at section A (Figure 2) can be explained partly by the cabbelling effect.

[13] At section G (Figure 2), which was surveyed 3 days after section A, both water temperature and salinity increased oceanward. The density was largest near the bottom layer, above which the density was high at station G8 and decreased oceanward. No similar frontal region as that observed at section A can be identified at section G. Since the thermohaline properties of section G were similar

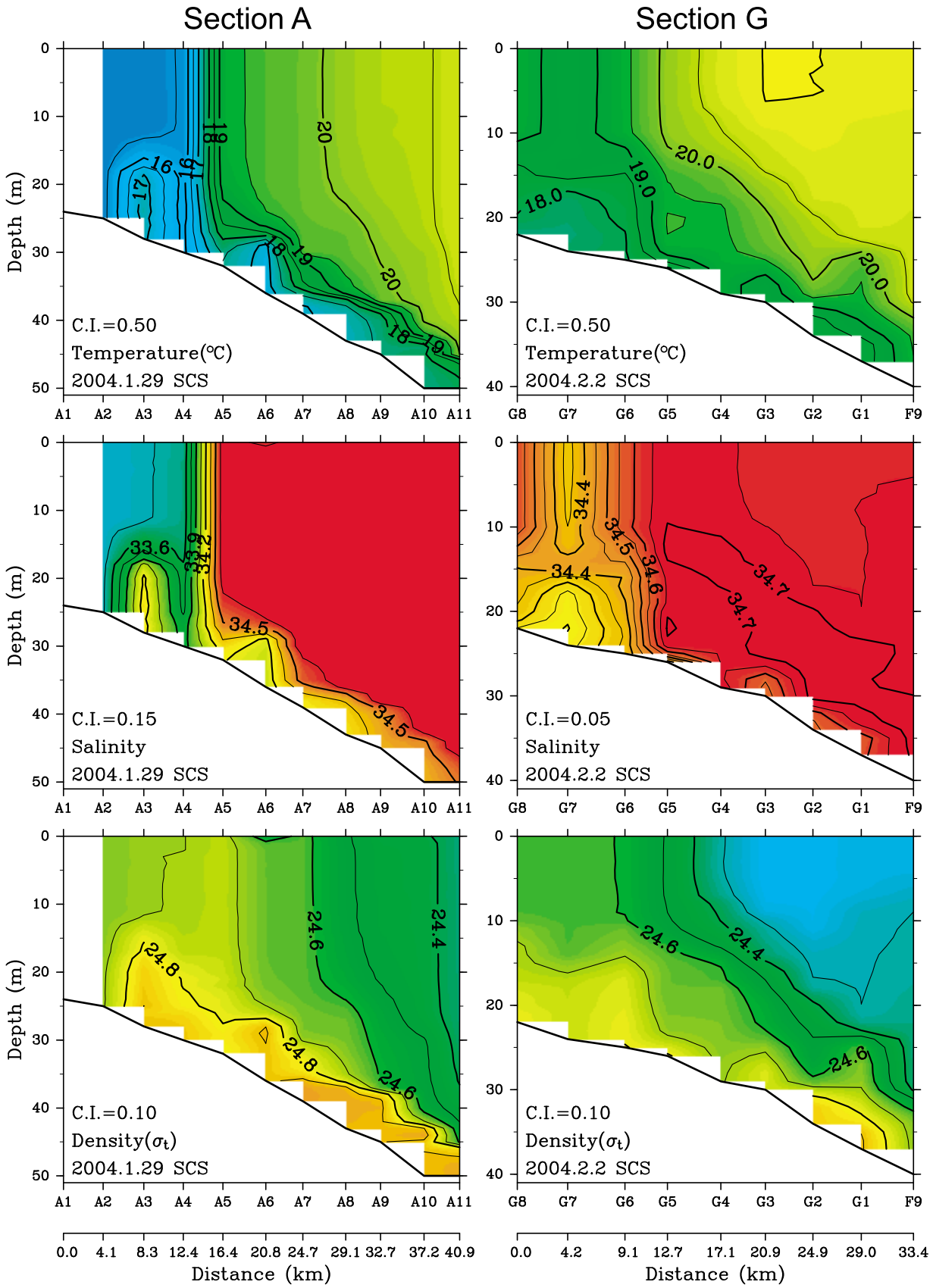

Figure 2. Vertical distributions of water temperature, salinity, and density along sections A and G in winter 2004. Note that there were no data at station A1 along section A because of a CTD malfunction.

to those observed on the front offshore side at section A, we suggest that there was an onshore movement of the front.

[14] With the sea surface temperature (SST) image from satellite, we can confirm the onshore and offshore movements of the front (Figure 3a). In all the available satellite images, an apparent SST front parallel to the coast can be identified. The front is not in a straight line, and the meandering of the front is found in the images. In our survey area, the front was sometimes far from the coast (e.g., 29 December 2003) or sometimes close to the coast (e.g., 6 January 2004). If all the front positions are overlapped in one single image (Figure 3b), the onshore and offshore movements of the front become more apparent. Although the satellite images in Figure 3 were not from the same day as our hydrographic observations, the season was the same. Therefore, the onshore movement of the front deduced from Figure 2 is reasonable.

3.2. Spatial Variation of Nutrients

[15] The distributions of inorganic and organic nutrients for the two studied sections are presented in Figure 4. For section A, the thermohaline front was also clearly observed on the inorganic nutrient distributions between stations A3 and A5. In general, concentrations of dissolved inorganic nutrients decreased from coastal (approximately 3.5 μM NO_3^-, 0.25 μM PO_4^{3-}, 7.0 μM $Si(OH)_4$) to oceanic (approximately 0.1–0.2 μM NO_3^-, 0.08 μM PO_4^{3-}, 1.6 μM $Si(OH)_4$) waters with 20-fold differences for NO_3^- and NO_2^- and fourfold differences for PO_4^{3-} and $Si(OH)_4$. The concentrations of NO_3^-, NO_2^-, PO_4^{3-}, and $Si(OH)_4$ were lower in the bottom layer than in the upper layer of the front onshore side, while they were higher in the bottom layer than in the upper layer of the front offshore side. The concentrations of NH_4^+, DON, and DOP do not have such a spatial distribution. One or more patches with high or low concentrations were found for these variables.

[16] The inorganic nutrient concentrations at section G were generally lower than those at section A, except for NH_4^+. The concentrations of NO_3^- and NH_4^+ decreased oceanward, and they increased from surface to bottom with a fivefold vertical difference for NO_3^-, a threefold difference for NO_2^-, and a onefold to twofold difference for PO_4^{3-} and $Si(OH)_4$. The DON and DOP concentrations showed patchy distributions with concentrations of 2–8 μM for DON and 0.04–0.1 μM for DOP.

3.3. Daily Nutrient Variations

[17] To examine daily nutrient variations, 25 h observations were performed at stations A3 and A6. At both stations, high temperatures (>19°C) and salinities (>34.5) were recorded, which were characteristic of the waters on the front offshore side (Figure 2). Here we show the data at station A6 to confirm the daily variations in nutrient concentrations (Figure 5). The data at station A3 were similar to those at station A6 and therefore not presented here.

[18] At station A6, NO_3^-, NO_2^-, and DOP varied daily by approximately tenfold, and NH_4^+, PO_4^{3-}, $Si(OH)_4$, and DON varied twofold to sixfold. Nutrient concentrations showed vertically well-mixed distributions, with the exception of dissolved silicate, which was higher in the bottom layer than in the upper layer. NH_4^+ accounted for 70%–90% of DIN, with an average of 80%. DON composed 70%–90% of TDN, with an average of ~80%. PO_4^{3-} represented 35%–90% of TDP, with an average of 60%.

4. Discussion

4.1. Nutrient Composition

[19] Nutrient concentrations in the study region, except for that of ammonium, were quite low compared to those in other Chinese coastal areas (i.e., the Bohai Sea, Yellow Sea, and East China Sea) [*Zhang and Su*, 2006]. Dissolved inorganic nutrients decreased oceanward, while DON and DOP showed patchy distributions, indicating a stronger, controlled by biological activity. High NH_4^+ and NO_2^- concentrations at the coastal stations are most likely related to decomposition of organic matter [*Cai et al.*, 2004] and river inputs. The proportion of PO_4^{3-} to TDP decreased from coastal (65–90%) to oceanic (30–75%) waters along section A, from 20% to 75% along section G, and ~50% at anchor station A6, indicating that PO_4^{3-} was rapidly removed and/or consumed within the oceanic waters and organic matter degradation increased oceanward, replenishing phosphate. The molar ratios of $NO_3^-/(NH_4^+ + DON)$ also decreased from coastal (0.6) to oceanic (<0.05) waters along section A, 0.01–0.05 along section G, and <0.08 at anchor station A6, indicating the importance of regenerated nitrogen (NH_4^+ + DON) in sustaining primary production. With respect to nutrient composition, NH_4^+ was the major component of DIN, and the highest contribution of TDN corresponded to DON.

[20] There are remarkable correlations among the nutrient concentrations with a correlation coefficient (R) for DIN versus PO_4^{3-} of 0.76, R for $Si(OH)_4$ versus DIN of 0.87, and R for $Si(OH)_4$ versus PO_4^{3-} of 0.85 at $p = 0.001$, $n = 123$. The mean molar ratio from all the data was 19 for DIN/PO_4^{3-}, 0.91 for $Si(OH)_4$/DIN, and 23 for $Si(OH)_4/PO_4^{3-}$, respectively. Nitrogen and/or silicon limitation was reported in the northern SCS [*Lee Chen and Chen*, 2006; *Zhang et al.*, 1999]. However, the mean molar ratios from our study indicate that phosphorus may be the limiting nutrient for phytoplankton growth with the condition that phosphate concentrations are under their limiting values [*Ning et al.*, 2004; *Xu et al.*, 2008]. Previous incubation experiments indicated that phosphate was the limiting element in the Zhujiang riverine effluent plume [*Zhang et al.*, 1999]. It was reported that the Zhujiang river has a very high DIN input, resulting from fertilizer usage, and high dissolved silicate concentrations, reflecting the drainage basin mineralogy, but it has a relatively low phosphate input [*Cai et al.*, 2004; *Zhang et al.*, 1999].

[21] Spatially, as water temperature increased, NO_3^-, NO_2^-, PO_4^{3-}, and $Si(OH)_4$ concentrations decreased significantly, that of NH_4^+ decreased slightly, and those of DON and DOP had no trends (Figure 6a). Apparently, there were high dissolved inorganic nutrient levels in coastal waters with temperature <16°C. Their concentrations decreased significantly as water temperature increased to 18°C, reflecting the dominant role of the thermohaline front along section A. In addition, the biological activities also affect the variation of nutrients with temperature.

[22] Plotting nutrient concentrations versus salinity indicated that dissolved inorganic nutrient concentrations decreased as salinity increased (Figure 6b). The linear cor-

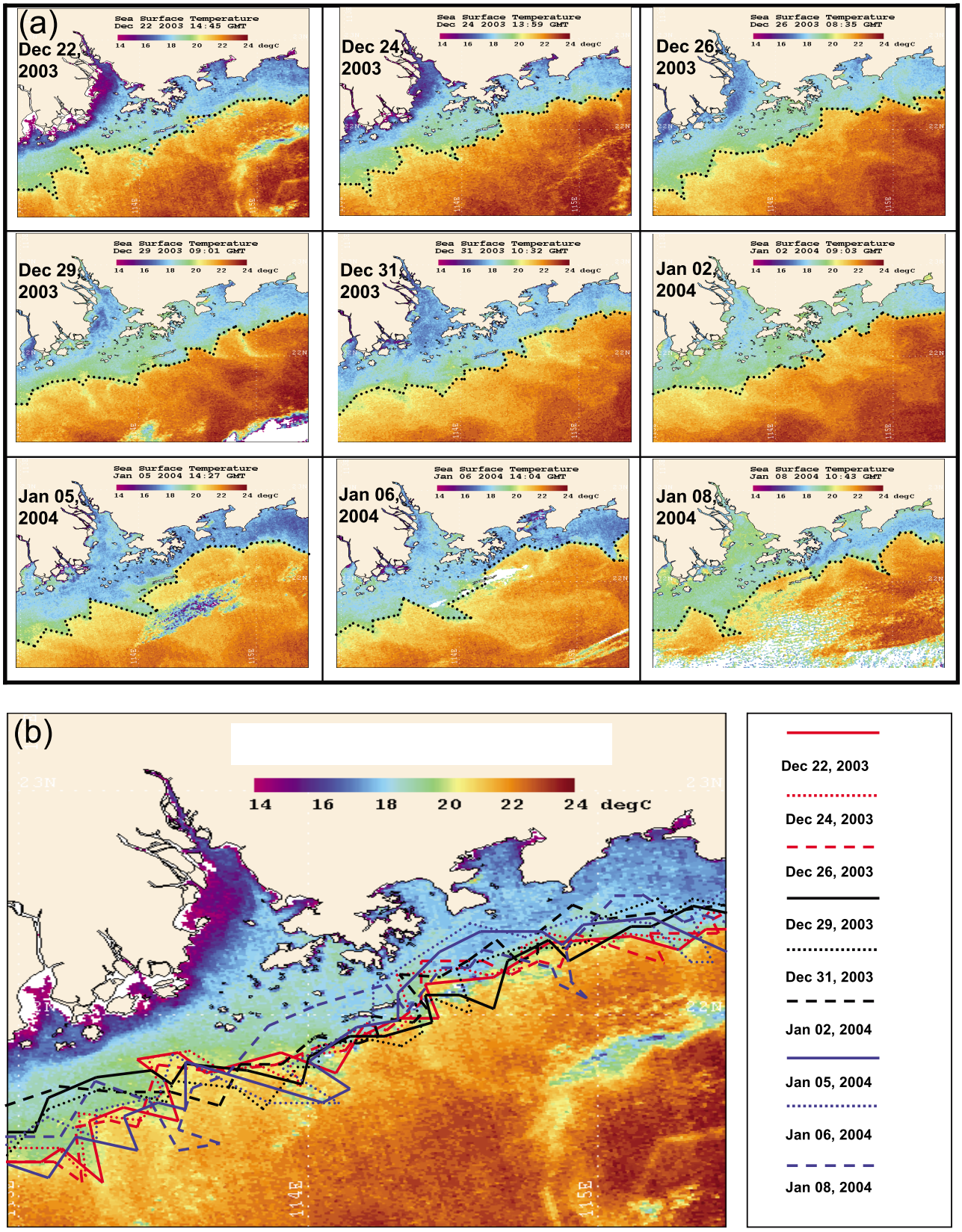

Figure 3. (a) Advanced very high resolution radiometer infrared images of the northern part of the South China Sea between 22 December 2003 and 8 January 2004 (courtesy of J.-C. Chen, Center for Astrodynamics Research, Hong Kong University of Science and Technology). The dotted line in each panel denotes position of front. (b) Composite infrared image overlapping all the front positions between 22 December 2003 and 8 January 2004.

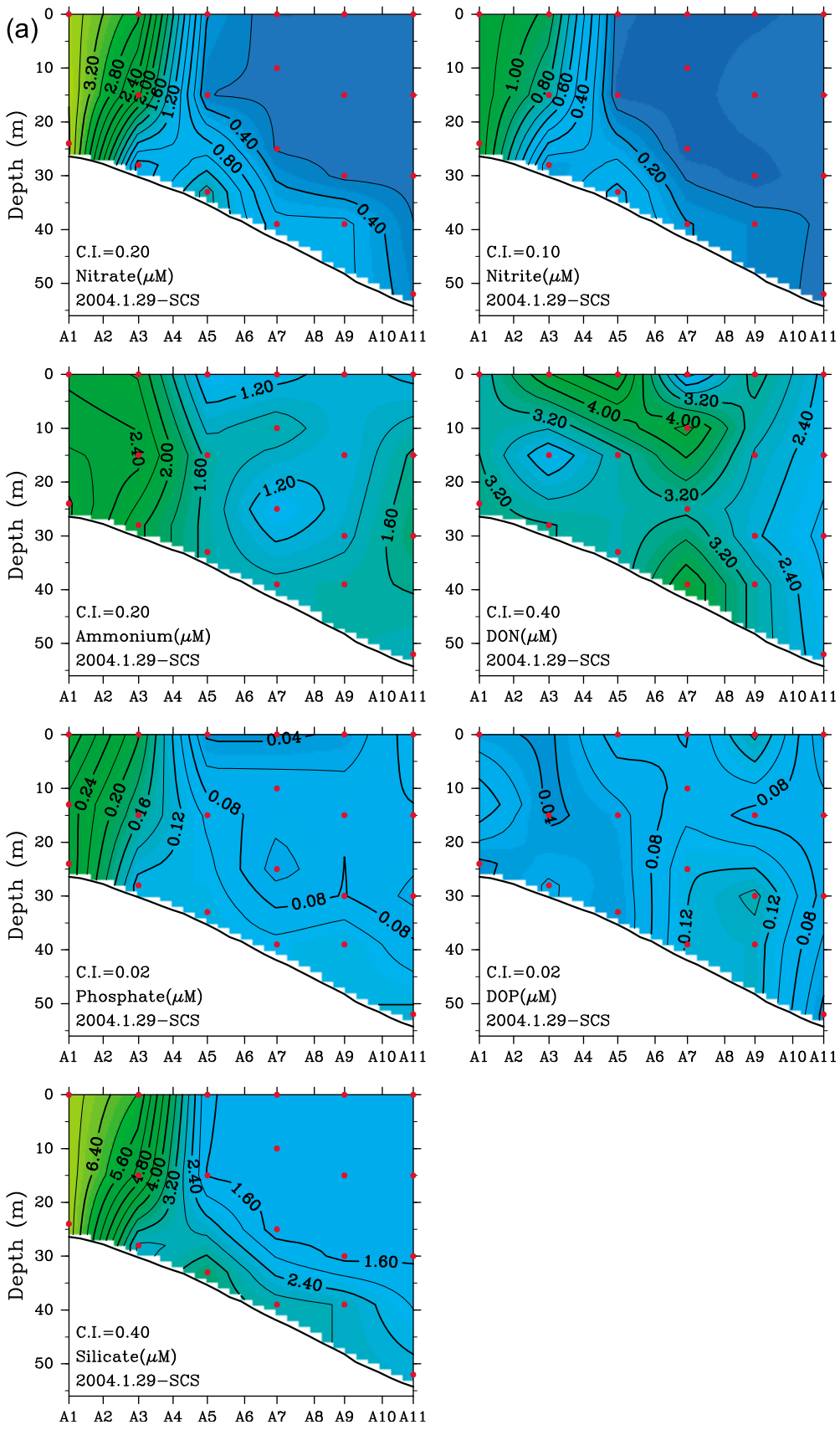

Figure 4. Vertical nutrient distributions (NO_3^-, NO_2^-, NH_4^+, PO_4^{3-}, $Si(OH)_4$, DON, and DOP) for sections (a) A and (b) G in winter 2004. The red dots denote the depths of water samples for nutrient analysis.

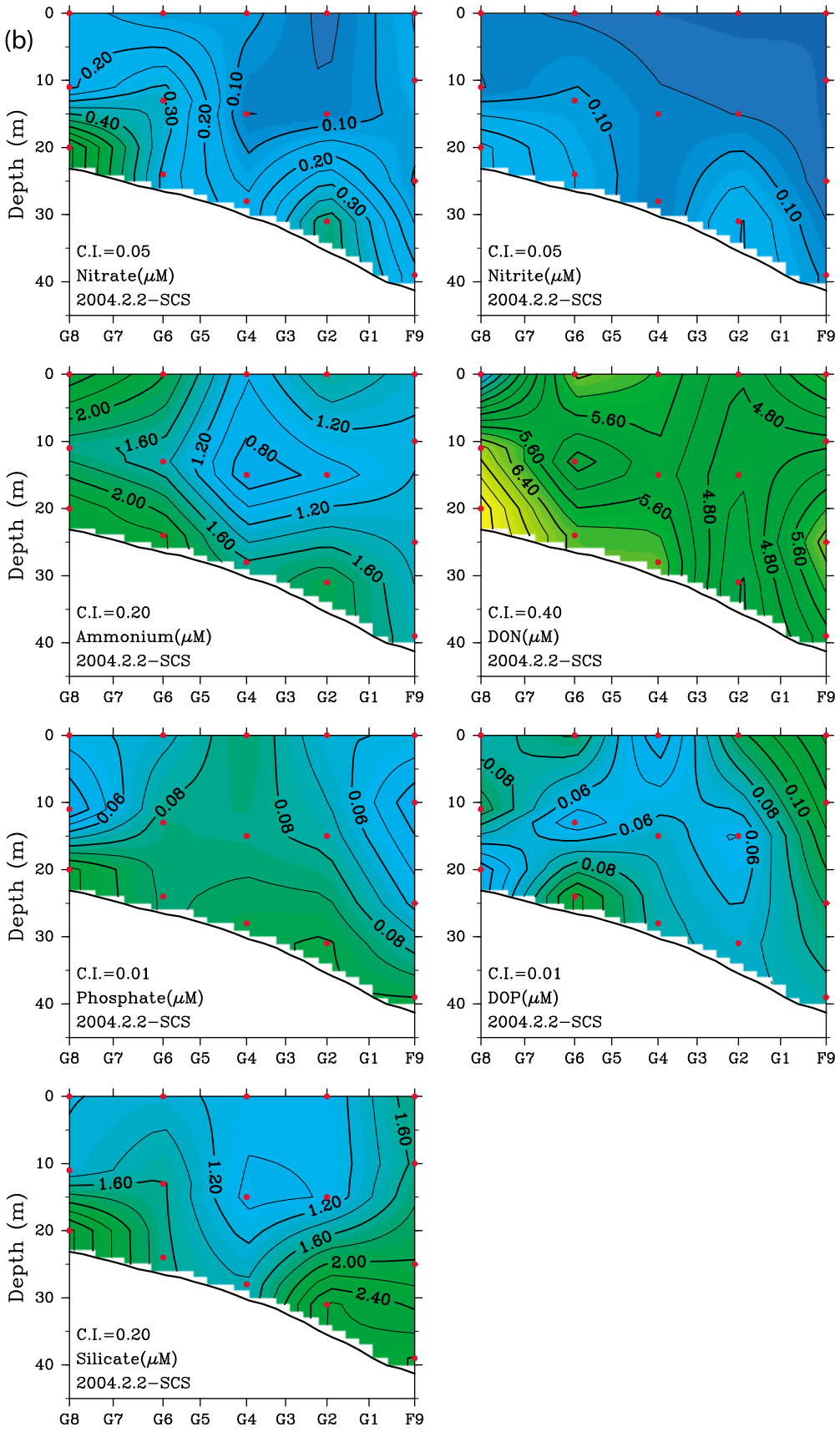

Figure 4. (continued)

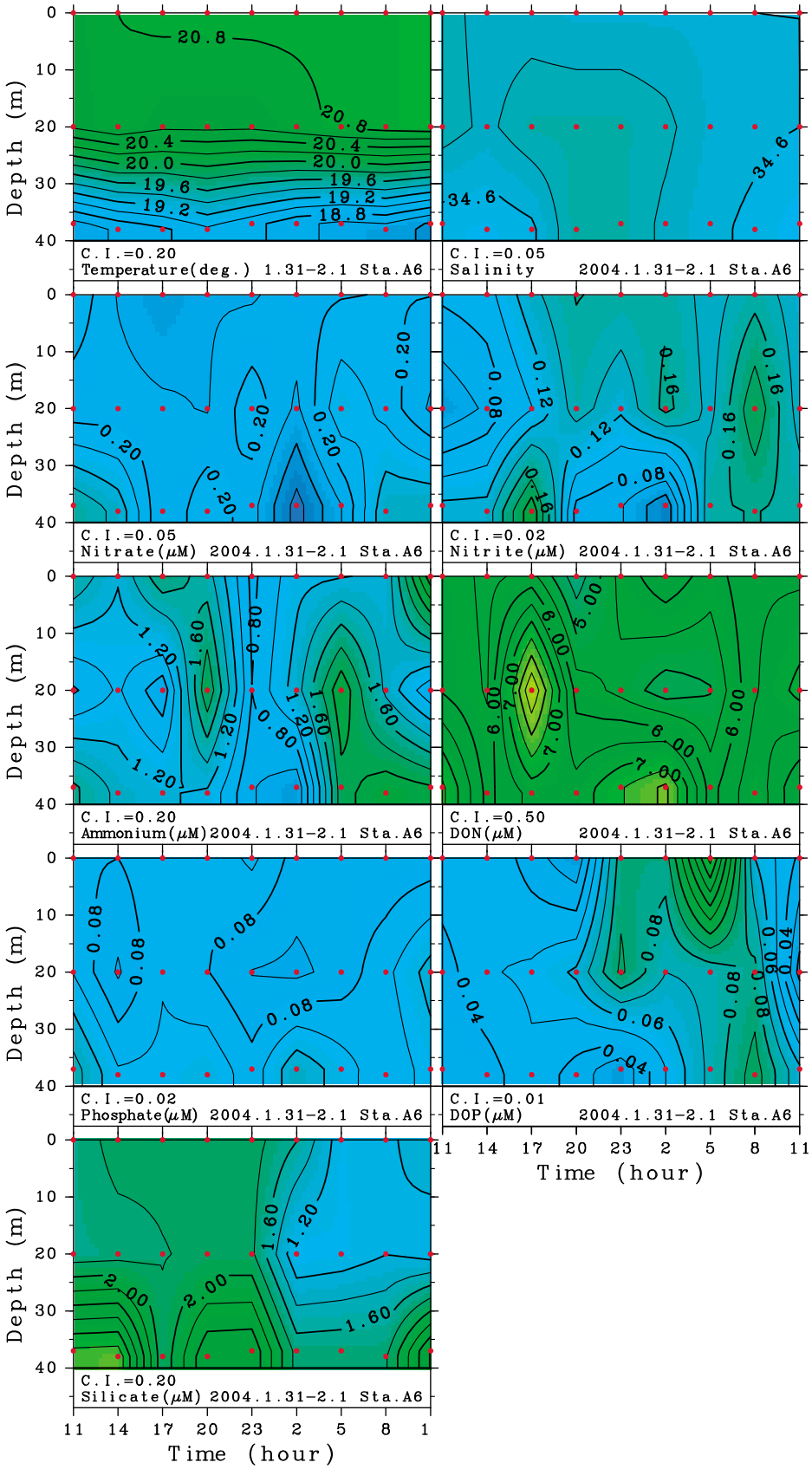

Figure 5. Temporal variation of temperature, salinity, and nutrients (NO_3^-, NO_2^-, NH_4^+, PO_4^{3-}, $Si(OH)_4$, DON, and DOP) at anchor station A6 in winter 2004. The red dots denote the depths of water samples for nutrient analysis.

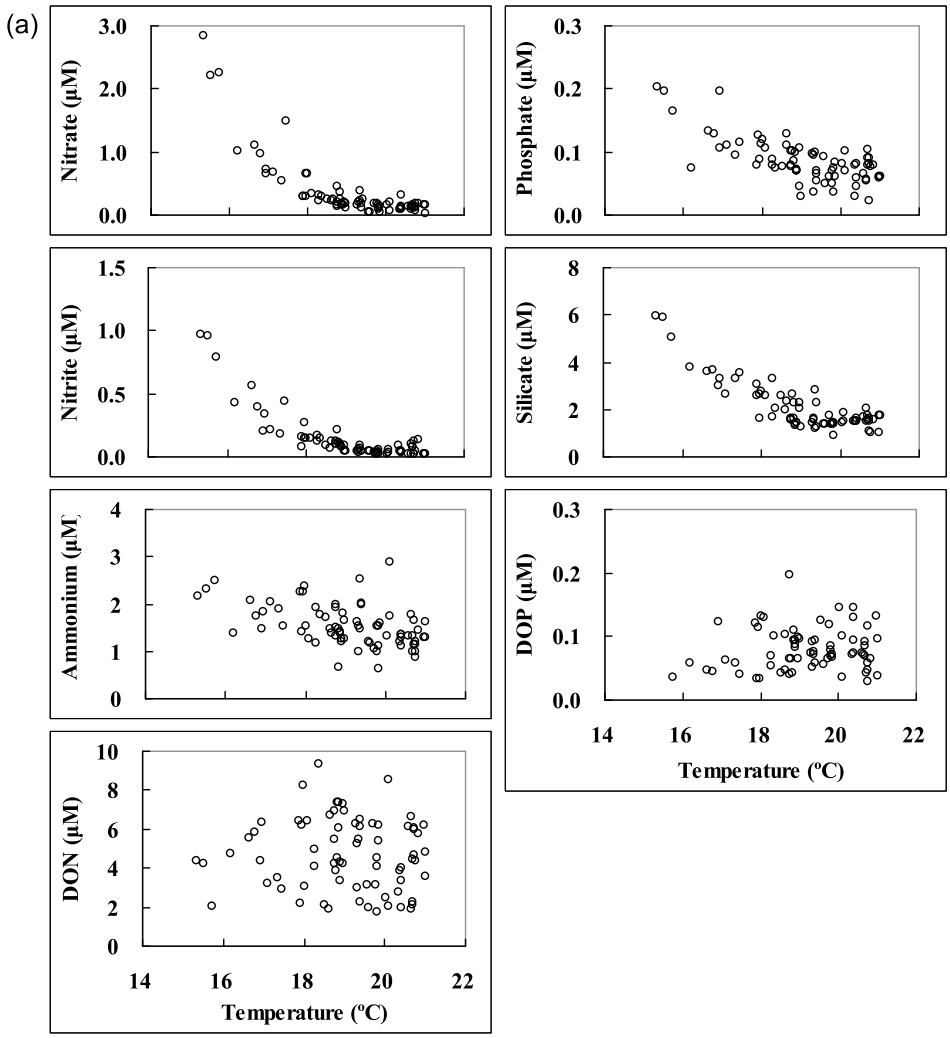

Figure 6. Plots of nutrient concentrations (μM) versus (a) water temperature and (b) salinity; shown are all data for all stations in the four sections in winter 2004.

relations are significant at the 95% confidence level, and the correlation coefficients range from 0.41 to 0.90 (n = 74), suggesting that terrestrial input (nonpoint discharge) is the major cause of high dissolved inorganic nutrient levels in coastal waters. On the other hand, the DON and DOP concentrations were not correlated with salinity, pointing to a stronger biological control on the organic nutrient levels.

4.2. Nutrient Transport in the Thermohaline Frontal Zone

[23] Fronts play an important role in water exchange and, consequently, in the exchange of dissolved and suspended matters [*Jakobsen*, 1997; *Brandini et al.*, 2000]. Since current data are available for the two sections along which nutrients were measured, nutrient fluxes can be obtained by multiplying the velocity and the nutrient concentrations. With the calculated nutrient fluxes, we can examine the influence of the thermohaline front on nutrient transports by comparing the nutrient fluxes in the presence (such as section A) and absence (such as section G) of the thermohaline front.

[24] The thermohaline front in the SCS is reported to be oriented along the coast [*Wang et al.*, 2001], generally parallel to the isobaths (Figure 3). To examine nutrient transport along and across the front, we calculated along-isobath component and across-isobath component of the velocity and nutrient flux. The positive direction for along-isobath component is 30°T (clockwise 30° from north), or northeastward along the coast, while that for across-isobath component is 120°T (clockwise 120° from north), or southeastward perpendicular to the coast.

[25] Before we discuss nutrient transport along the two sections (A and G), we need to examine the contamination attributed to tidal currents. Tidal currents are periodic oscillations and do not contribute to the nutrient fluxes with time scales longer than the tidal period (~1 day or longer). However, nutrient transport caused by tidal currents is actually included in any snapshot observation of currents like ours along these two sections in the SCS. If tidal currents are very weak like they are in the deep open ocean, their influence on the flux estimate from snapshot current data can be neglected; if the tidal currents are of the same order as or stronger than the subtidal currents, their influence cannot be neglected.

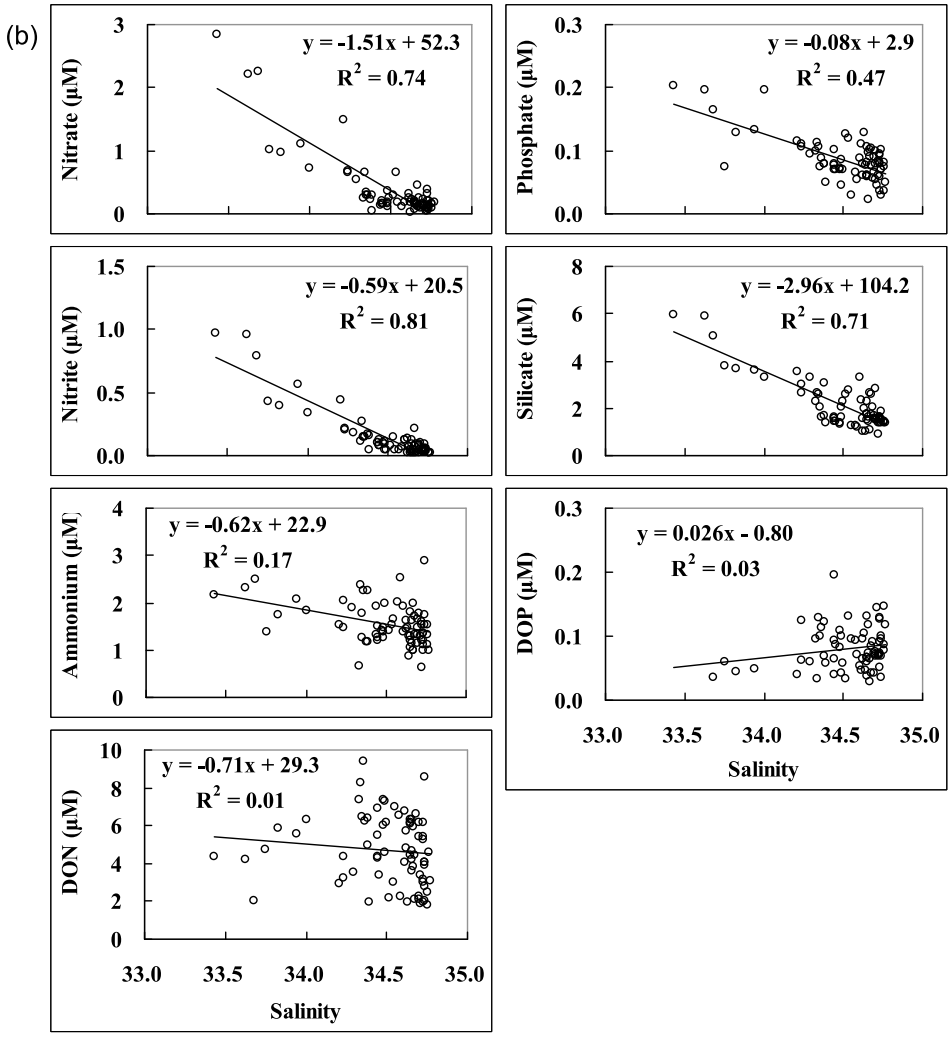

Figure 6. (continued)

[26] Removing tidal influences from snapshot current data is not easy. A numerical tidal current model [*Foreman and Freeland*, 1991] or fitting tidal currents with a mathematical function [*Candela et al.*, 1992] provides possibilities for detiding such snapshot current data. However, validating tidal currents predicted by a numerical model is difficult, and the precision of the functional fit of tidal currents is still questionable [*Carrillo et al.*, 2005]. Here, instead of detiding the snapshot current data, we examine the extent of tidal current contamination on the nutrient fluxes estimated from the snapshot data in our study area.

[27] At the two anchor stations, currents were measured every hour for 25 h. Such current data allow a direct harmonic analysis of the tidal currents by assuming

$$u(t) = u_0 + u_1 \cos(\omega_1 t - \alpha_1) + u_2 \cos(\omega_2 t - \alpha_2) + \varepsilon(t), \quad (1)$$

where u is eastward or northward velocity; t is time; u_0 is constant during the anchor period (hereafter called subtidal current); u_1, ω_1, and α_1 are the amplitude, frequency, and phase of the diurnal tidal constituent represented by the K_1 constituent; u_2, ω_2, and α_2 are the amplitude, frequency, and phase of the semidiurnal tidal constituent represented by the M_2 constituent; and ε denotes the residual. With least squares method to minimize total ε^2 from all the hourly data measured at one anchor station, u_0, u_1, α_1, u_2, and α_2, can be obtained.

[28] Figure 7 shows the vertical profiles of the across- and along-isobath components of the subtidal current and the profiles of the diurnal and semidiurnal tidal current amplitudes at stations A3 and A6. The subtidal currents, both the across-isobath component and the along-isobath component, are larger than the tidal current amplitudes at the two stations. Within the tidal currents, the diurnal tidal constituent is stronger than the semidiurnal one at station A3 except for the bottom 3 m, but they are comparable at station A6.

[29] The nutrient fluxes caused by the subtidal currents at stations A3 and A6 and the ratio of fluxes attributed to the tidal currents to those resulting from the subtidal currents are presented in Table 1. The ratio can be considered an index indicating the contamination from the tidal currents in the flux estimate caused by the subtidal currents using a snapshot current field. This index is calculated by $\frac{1}{N}\sum_{i=1}^{N}\frac{|V_T(t_i)C(t_i)|}{|V_0C(t_i)|}$,

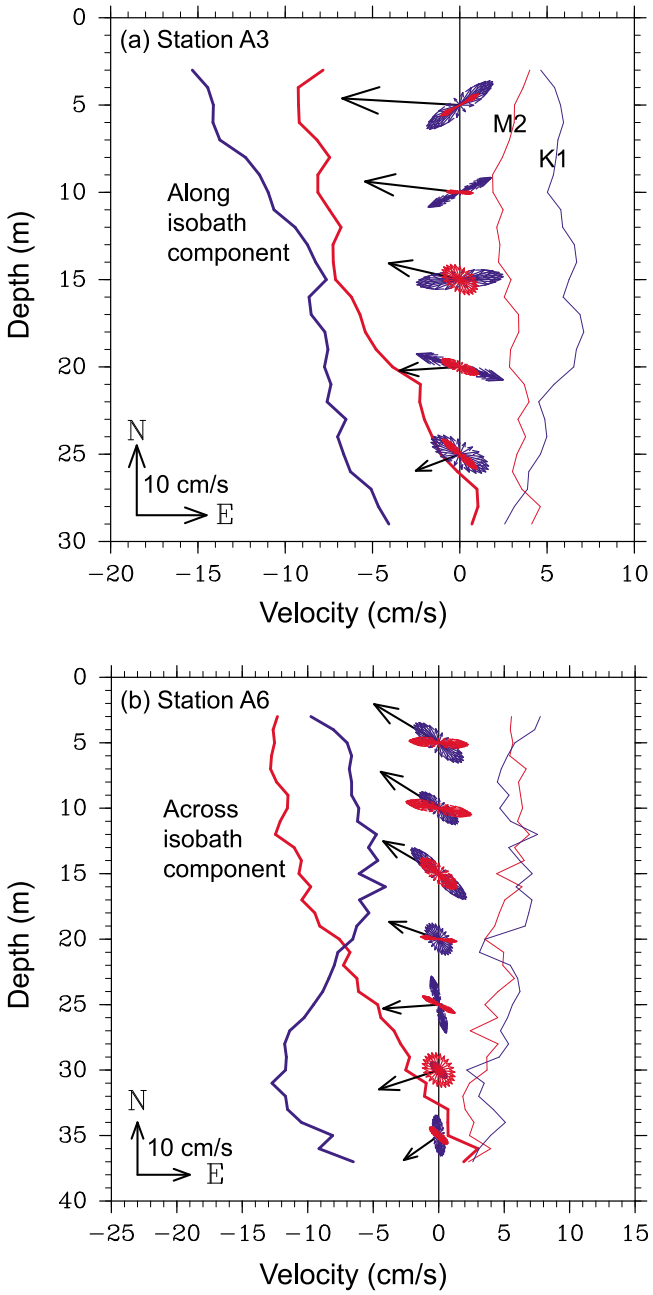

Figure 7. Subtidal current (arrows), its across-isobath component (thick red line) and along-isobath component (thick blue line), amplitudes of diurnal tidal (thin blue line) and semidiurnal tidal (thin red line) currents, and their tidal ellipses at anchor stations (a) A3 and (b) A6. The tidal ellipse colors correspond to the tidal current amplitudes.

where i is the number of data, N is the total number of data for the anchor period, t_i is the time of measurement, $C(t_i)$ is the concentration of nutrient species at time t_i, $V_T(t_i)$ is the tidal current predicted by $V_T(t_i) = u_1 \cos(\omega_1 t_i - \alpha_1) + u_2 \cos(\omega_2 t_i - \alpha_2)$, and V_0 is the subtidal current. The value of this index varies within a range of 0.2–0.5 (Table 1), indicating that the uncertainty in the fluxes estimated from the snapshot current field is acceptable in our study area, where the tidal currents are not strong enough to change the direction of nutrient fluxes because of the subtidal currents. Therefore, the calculated nutrient fluxes from the snapshot current data along sections A and G can be considered to be qualitatively accurate and quantitatively acceptable with an uncertainty of 20%–50% in the values.

[30] At section A, the cross-isobath velocity component in the upper layer (shallower than 20 m) was positive on the thermohaline front onshore side (stations A3 and A4) and negative on the front offshore side (Figure 8a), indicating convergence of surface waters toward the thermohaline front between stations A4 and A5 (Figure 2). In the lower layer, the cross-isobath velocity component was positive for both the onshore side and offshore side of the front. Such a flow structure suggests that the downwelled waters and material attributed to surface water convergence at the front were transported to the lower layer of the front offshore side, forming a pathway for offshore transport of coastal material.

[31] The across-isobath velocity at section G was either positive or negative in the vertical direction, showing a possibility of convergence in the entire water column (Figure 8b). Since no clear thermohaline front can be identified along section G (Figure 2) and the across-isobath velocity is almost homogeneous in the vertical direction (Figure 8b), this convergence may be attributed to the onshore movement of the front.

[32] The along-isobath velocity component is negative (i.e., southwestward) over almost the entire area of section A (Figure 8c). Its vertical variation is small, showing a strong barotropic character. Horizontally, it is strong on the shallow onshore side (~0.2 m/s) and weak on the deep offshore side (~0.05 m/s). The along-isobath velocity at section G was also generally negative, but positive and negative along-isobath velocity components coexist in the upper layer of the offshore side (Figure 8d).

[33] The southwestward coastal current appearing as a negative along-isobath component at sections A and G (Figures 8c and 8d) is consistent with the South China Sea coastal current that is dominated by the northeasterly monsoon [*Su*, 1998]. The relaxation or intensification of the northeasterly wind naturally modifies the current's strength and location, which in turn results in the onshore or offshore movement of the thermohaline front (Figure 3). The spatial distribution of along-isobath component at sections A and G (Figures 8c and 8d) suggests that this current is stronger at the onshore side than at the offshore side.

[34] The direction of the nutrient fluxes depends on the flow direction, while the magnitude of nutrient fluxes depends not only on the flow speed but also on the nutrient concentrations. As an example, the across- and along-isobath nitrate fluxes at sections A and G are presented in Figure 9. As expected from the nitrate concentrations (Figure 4) and the across- and along-isobath flow components (Figure 8), the nitrate flux is large at the onshore side of two sections and small at the offshore side, where the nitrate concentration is low. The nitrate fluxes are relatively larger at section A.

[35] At section A, the positive across-isobath fluxes at the front onshore side and in the bottom layer of the front offshore side are significantly larger than the negative across-isobath fluxes in the surface layer of the front offshore side (Figure 9a). This suggests that the nitrate transported oceanward in the bottom layer of the front offshore side

Table 1. Vertically Integrated Flux Across and Along Isobaths at the Two Anchor Stations A3 and A6[a]

	Vertically Integrated Flux Across Isobath		Vertically Integrated Flux Along Isobath	
	Flux Caused by the Subtidal Current	Ratio of Flux Caused by the Tidal Current to That Caused by the Subtidal Current	Flux Caused by the Subtidal Current	Ratio of Flux Caused by the Tidal Current to That Caused by the Subtidal Current
Station A3				
Velocity	−1.510	0.293	−2.813	0.270
NO_3^-	−0.194	0.318	−0.394	0.267
NO_2^-	−0.064	0.515	−0.137	0.266
NH_4^+	−2.503	0.295	−4.730	0.273
DON	−6.197	0.292	−11.458	0.275
PO_4^{3-}	−0.099	0.387	−0.198	0.271
DOP	−0.105	0.263	−0.196	0.282
$Si(OH)_4$	−2.214	0.389	−4.496	0.271
Station A6				
Velocity	−2.622	0.464	−3.215	0.210
NO_3^-	−0.475	0.520	−0.647	0.189
NO_2^-	−0.333	0.464	−0.401	0.212
NH_4^+	−3.428	0.464	−4.243	0.208
DON	−15.587	0.484	−20.068	0.202
PO_4^{3-}	−0.213	0.497	−0.295	0.196
DOP	−0.160	0.444	−0.184	0.219
$Si(OH)_4$	−4.013	0.523	−5.764	0.189

[a]The method for calculating the fluxes and the ratio is described in section 4.2. The unit of velocity flux (i.e., volume transport through a unit width) is $m^2\ s^{-1}$, and the unit of other quantities is $\mu M\ m^2\ s^{-1}$.

originates mainly from the front onshore side (i.e., from coastal waters).

[36] For a quantitative discussion on nutrient transports, the across- and along-isobath fluxes for all nutrients were then integrated from bottom to surface at all stations along two sections, and the results are presented in Tables 2 and 3. The offshore transports of nutrients were larger at stations A3 and A4 and decreased by 1 order at the offshore stations (Table 2). The offshore transports of nutrients could also be found at some stations along section G, but the magnitude of transports were smaller than those near the thermohaline front such as stations A3 and A4 by 1 order (Table 2).

[37] In general, the direction of vertically integrated fluxes is consistent with that of the vertically integrated velocity, indicating a vertically homogeneous distribution of nutrients and current, just like on the shallow shelf in winter (Table 2). However, this consistency does not hold at the thermohaline front offshore side (stations A5 and A6) for the across-isobath nitrate and nitrite fluxes (Table 2). The cause for this inconsistency is apparent: the two nutrient concentrations were high in the lower layer and extremely low in the upper layer while the across-isobath velocity was opposite in the upper and lower layers (Figures 8 and 9).

[38] As previous numerical studies suggested [*Akitomo et al.*, 1990], the surface water converges at a thermohaline front, sinks there, and diverges at the bottom layer. As this idea is extended to material transport, the concentrations of material on the onshore and offshore sides of the front become important. In our study, the converging waters from the front offshore side contains few nutrients (Figure 4), and therefore the nutrients inside the diverging waters at the bottom layer must come mainly from the inner shelf, where the terrigenous input is the major source of nutrients. Consequently, the presence of the thermohaline front in the northern SCS in winter promotes the offshore transport of terrigenous nutrients.

[39] The along-isobath nutrient transports at all the stations along two sections were mainly southwestward, and their values were usually larger than the across-isobath nutrient transports by 1 order (Table 3). The Zhujiang river is a major source of riverine nutrients to the northern shelf of the SCS [*Lee Chen and Chen*, 2006; *Zhang et al.*, 1999]. Our survey area is located northeast of the Zhujiang river mouth. It is possible for the Zhujiang diluted waters to affect our survey area in summer but not in winter, because the strong southwestward coastal current in winter tends to push the Zhujiang diluted waters southwestward. On the other hand, nutrients from the East China Sea transported by southwestward coastal currents in winter through the Taiwan Strait have recently been suggested to contribute to the northern shelf of the SCS, although the exact nutrient flux through the Taiwan Strait in winter is still unknown [*Chen*, 2008].

[40] To understand the role of thermohaline front in nutrient transports on the northern shelf of the SCS, we compare the offshore fluxes across the thermohaline front in the SCS with the nutrient fluxes from the Changjiang and Zhujiang rivers. The Changjiang river is the largest source of terrigenous nutrients in the ECS while the Zhujiang river is the largest one in the SCS.

[41] The wintertime nutrient fluxes from the Changjiang river have been estimated to be 765 mol s^{-1} for nitrate, 23.9 mol s^{-1} for nitrite, 195 mol s^{-1} for ammonium, 6.0 mol s^{-1} for phosphate, and 1366 mol s^{-1} for dissolved silicate, respectively [*Zhang et al.*, 2007]. The wintertime nutrient fluxes from the Zhujiang river into the SCS have been estimated to be 199.1 mol s^{-1} for nitrate, 7.1 mol s^{-1} for nitrite, 75.3 mol s^{-1} for ammonium, 2.3 mol s^{-1} for phosphate, and 363.4 mol s^{-1} for dissolved silicate, respectively [*Liu et al.*, 2009].

[42] To estimate the offshore flux across the thermohaline front, we need to know the length of the front. *Wang et al.* [2001] reported it to be about 700 km from infrared satellite

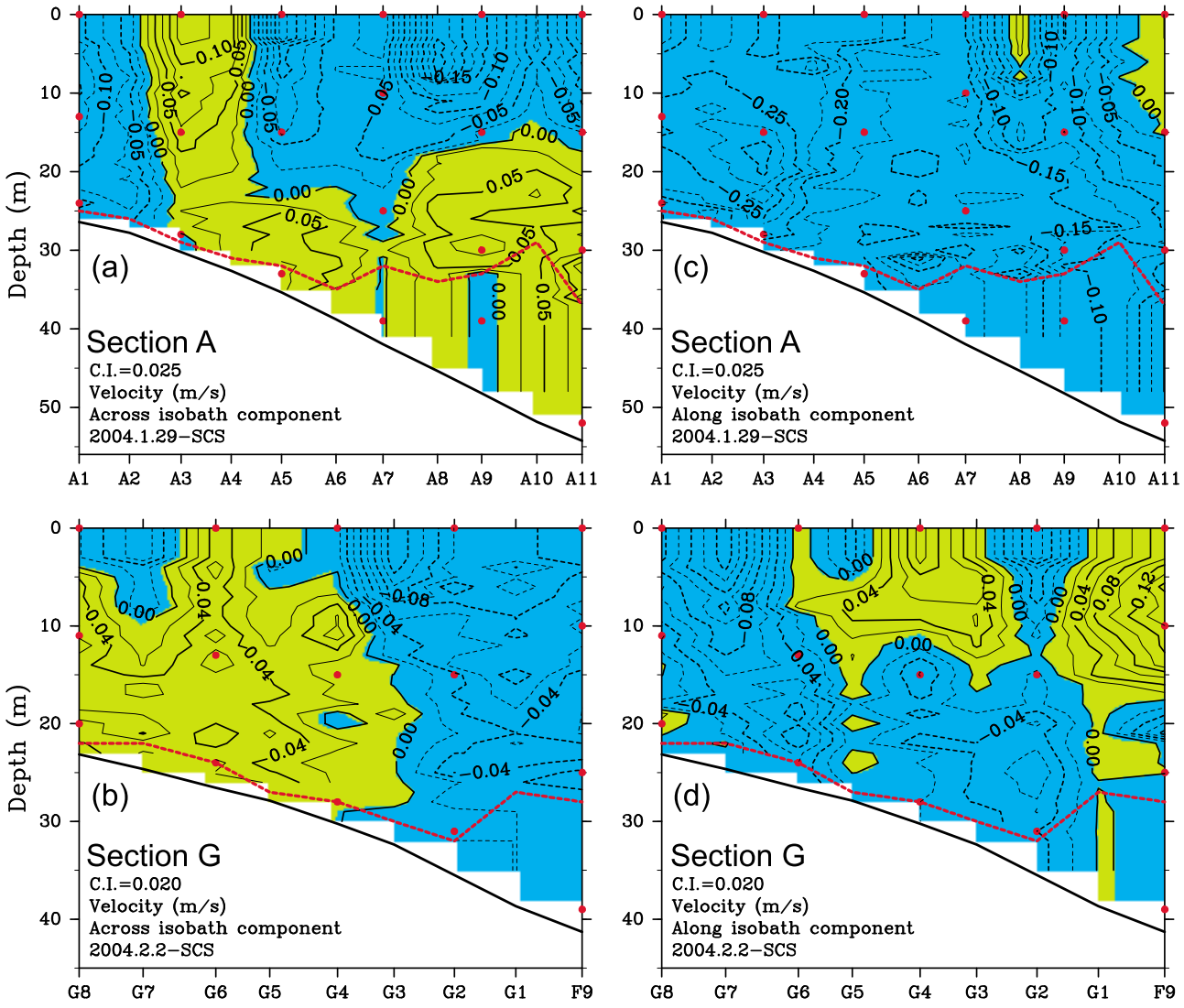

Figure 8. Across- and along-isobath velocity (m s^{-1}) components along sections (a and c) A and (b and d) G in winter 2004. Positive values indicate offshore and northeastward velocities; negative values indicate onshore and southwestward velocities. The red dots denote the depths of water samples, while the red dashed line indicates the deepest place between which and 3 m depth the ADCP data are available with a vertical interval of 1 m. The velocities at depths shallower than 3 m and deeper than the red dashed line were obtained by extrapolation.

image in wintertime. Referring to the values reported in Table 2 (e.g., those at station A11) and their 20%–50% uncertainty, and assuming 500 km as a low limit of the front length, it can be easily deduced that the seaward nutrient fluxes across the front are 178 mol s^{-1} for nitrate, 60 mol s^{-1} for nitrite, 1145 mol s^{-1} for ammonium, 50 mol s^{-1} for phosphate, and 1518 mol s^{-1} for dissolved silicate, respectively. These estimates have a large uncertainty since the meandering of and the movement of the front can result in a large spatial variability in offshore nutrient fluxes. Therefore, further field research using a higher-resolution sampling grid with more alongshore sections across the thermohaline front is necessary to give a more accurate estimate of the across-shore transport. These offshore fluxes are larger than the nutrient fluxes from the Zhujiang river and those from the Changjiang river except for nitrate. Although station A11 is far from the front, its offshore flux in the bottom layer apparently depends on the presence of the front (Figure 9a).

[43] The presence period of the thermohaline front in the northern SCS shelf has been reported from December to March [*Wang et al.*, 2001]. Such long presence time suggests that the offshore nutrient transports associated with the thermohaline front are important processes supporting high primary production in offshore waters of SCS in winter. At the same time, they are also important processes removing the nutrients accumulated in coastal waters.

5. Summary

[44] In the northern shelf of the SCS, the presence of a thermohaline front between coastal waters and oceanic waters was confirmed by a field observation in winter. High

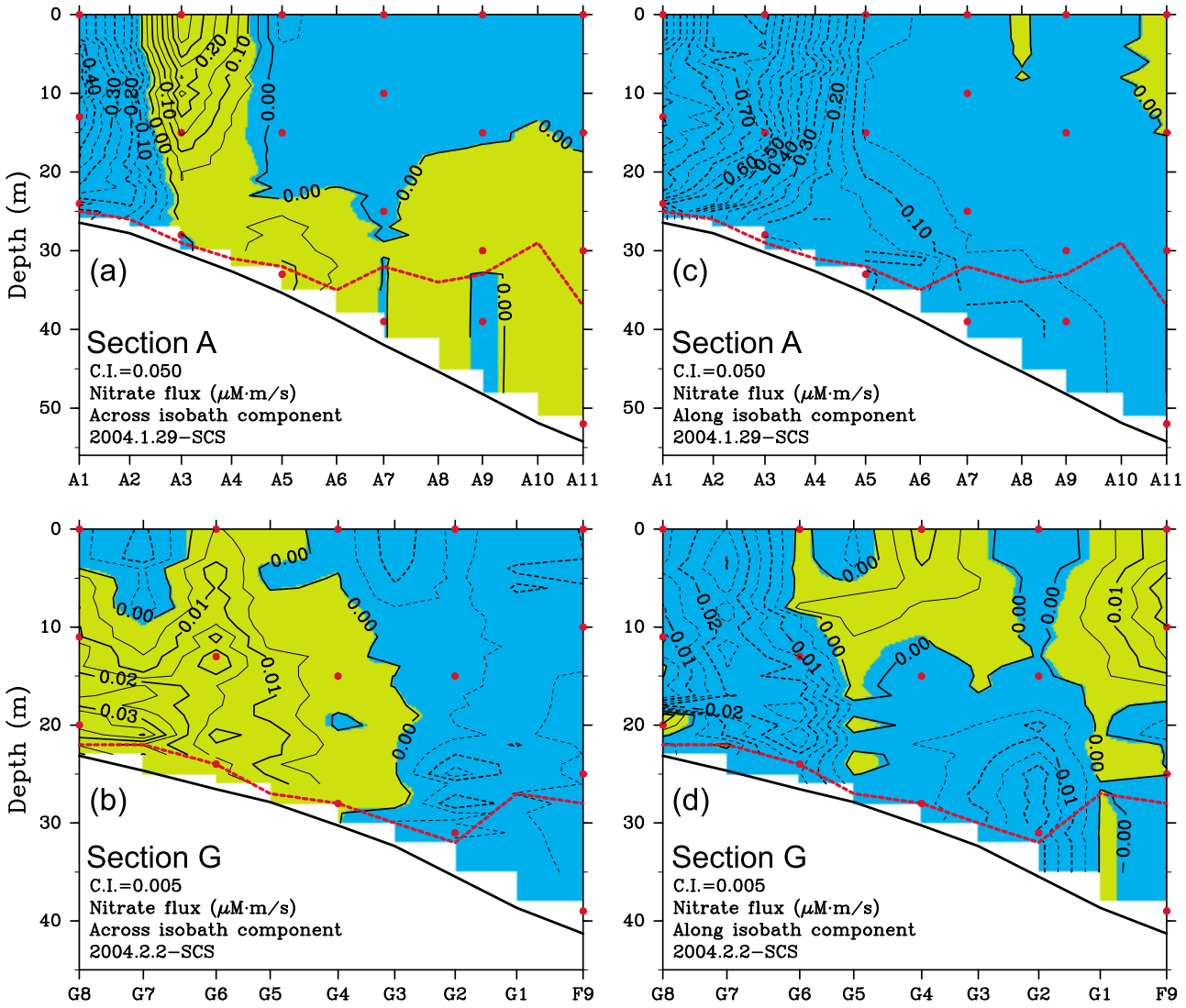

Figure 9. As in Figure 8 but for nitrate flux.

levels of dissolved inorganic nutrients were observed in the coastal waters with low temperature and salinity, while low levels of these nutrients were in oceanic waters with high temperature and salinity. Dissolved organic nutrients were patchily distributed, indicating a stronger, controlled by biological activity than by physical fields. There were high correlations ($R > 0.76$) among several major nutrient concentrations, while the mean molar ratios of DIN/PO_4^{3-} and $Si(OH)_4$/DIN were 19 and 0.91, respectively.

[45] The observations indicated that the presence of a thermohaline front along the continental shelf in winter promotes the offshore transport of nutrients from coastal waters. The transport pathway is the convergence of surface coastal waters to the front, downwelling at the front, and oceanward movement through the bottom layer of the front offshore side. The nutrient fluxes transported across the entire front in the SCS are estimated to be larger than those from the Zhujiang and the Changjiang rivers. This indicates the important role of thermohaline fronts in transporting riverine nutrients from the shallow inner shelf to the deep outer shelf in the SCS.

[46] There is an uncertainty of 0.2–0.5 in the nutrient flux values since tidal currents were not removed from the currents data used for the calculation of nutrient fluxes. However, the conclusion that the presence of a thermohaline front in the northern shelf of the SCS induces an offshore transport of nutrients is acceptable because the uncertainty of 0.2–0.5 does not change the flux direction. To obtain an estimate on the magnitude of total nutrient transports across the thermohaline front whose length was assumed as 500 km, we assumed the same offshore nutrient transports occurring along the entire front. This assumption has a large uncertainty since the meandering of and the movement of the front can result in a large spatial variability in offshore nutrient fluxes. Therefore, additional field research using the higher-resolution sampling grid with more alongshore sections across the thermohaline front is necessary to give a more accurate estimate of the across-shore transport. Moreover,

Table 2. Vertically Integrated Flux in the Across-Isobath Direction at All the Stations Along Sections A and G[a]

	Station						
	A1	*A2*	*A3*	*A4*	*A5*	*A6*	*A7*
Velocity	−3.035	−1.678	2.040	1.631	−1.376	−0.276	−0.984
NO_3^-	−10.864	−4.730	5.009	2.212	0.297	0.171	−0.166
NO_2^-	−3.575	−1.576	1.714	0.708	0.167	0.064	−0.024
NH_4^+	−7.790	−4.157	4.741	2.900	−1.504	−0.354	−1.288
DON	−9.550	−5.075	6.520	6.000	−6.700	−1.190	−3.791
PO_4^{3-}	−0.805	−0.355	0.365	0.198	−0.050	−0.007	−0.063
DOP	−0.215	−0.090	0.074	0.089	−0.124	−0.020	−0.096
$Si(OH)_4$	−21.369	−9.892	10.950	5.643	−1.006	0.006	−1.433
	A8	*A9*	*A10*	*A11*		*G8*	*G7*
Velocity	−2.015	−1.422	1.187	1.140		0.883	0.097
NO_3^-	−0.005	−0.250	0.338	0.355		0.352	0.174
NO_2^-	−0.043	−0.115	0.109	0.120		0.127	0.075
NH_4^+	−2.595	−1.820	1.897	2.290		1.757	0.181
DON	−6.512	−4.902	2.693	1.965		6.556	1.635
PO_4^{3-}	−0.086	−0.078	0.104	0.100		0.059	0.025
DOP	−0.178	−0.161	0.110	0.065		0.060	−0.003
$Si(OH)_4$	−2.408	−2.385	2.316	3.036		1.650	0.552
	G6	*G5*	*G4*	*G3*	*G2*	*G1*	*F9*
Velocity	1.429	0.697	0.473	−1.531	−1.741	−2.193	−1.678
NO_3^-	0.383	0.146	0.037	−0.104	−0.202	−0.271	−0.237
NO_2^-	0.150	0.067	0.025	−0.046	−0.113	−0.101	−0.053
NH_4^+	2.617	1.053	0.410	−1.748	−2.366	−2.800	−2.134
DON	7.915	3.938	2.680	−8.057	−7.763	−10.940	−9.459
PO_4^{3-}	0.115	0.061	0.041	−0.118	−0.130	−0.136	−0.090
DOP	0.108	0.053	0.030	−0.093	−0.121	−0.194	−0.181
$Si(OH)_4$	2.205	0.973	0.492	−1.585	−2.287	−3.383	−3.225

[a]Positive value means seaward. The unit of velocity flux (i.e., volume transport through a unit width) is $m^2\ s^{-1}$, and the unit of other quantities is $\mu M\ m^2\ s^{-1}$.

Table 3. Vertically Integrated Fluxes in the Along-Isobath Direction at All the Stations Along Sections A and G[a]

	Station						
	A1	*A2*	*A3*	*A4*	*A5*	*A6*	*A7*
Velocity	−6.588	−6.540	−7.999	−6.711	−6.281	−6.063	−6.953
NO_3^-	−23.604	−18.814	−15.742	−8.473	−3.808	−2.586	−1.872
NO_2^-	−7.763	−6.279	−5.372	−2.719	−0.958	−0.626	−0.427
NH_4^+	−17.008	−16.124	−18.328	−12.311	−8.725	−8.014	−8.876
DON	−20.821	−19.863	−23.608	−22.302	−22.499	−21.358	−25.498
PO_4^{3-}	−1.749	−1.406	−1.269	−0.816	−0.534	−0.451	−0.476
DOP	−0.444	−0.356	−0.342	−0.346	−0.372	−0.491	−0.728
$Si(OH)_4$	−46.399	−39.151	−37.023	−22.393	−13.373	−11.497	−12.301
	A8	*A9*	*A10*	*A11*		*G8*	*G7*
Velocity	−4.592	−6.278	−3.367	−1.060		−0.790	−2.233
NO_3^-	−1.465	−1.659	−0.830	−0.160		−0.155	−0.526
NO_2^-	−0.377	−0.493	−0.288	−0.100		−0.048	−0.179
NH_4^+	−5.992	−8.394	−5.138	−1.948		−1.697	−4.367
DON	−14.717	−17.971	−7.940	−2.009		−3.517	−11.905
PO_4^{3-}	−0.391	−0.529	−0.283	−0.059		−0.036	−0.139
DOP	−0.546	−0.743	−0.303	−0.080		−0.064	−0.167
$Si(OH)_4$	−8.792	−11.388	−6.216	−1.641		−0.987	−3.171
	G6	*G5*	*G4*	*G3*	*G2*	*G1*	*F9*
Velocity	−0.918	0.040	0.283	0.200	−1.876	0.939	1.723
NO_3^-	−0.302	0.023	0.036	−0.051	−0.360	0.095	0.250
NO_2^-	−0.130	0.011	−0.003	−0.020	−0.184	0.032	0.038
NH_4^+	−1.749	−0.011	0.214	0.022	−2.836	1.140	2.034
DON	−4.989	0.040	1.688	1.065	−8.112	4.589	8.831
PO_4^{3-}	−0.081	0.005	0.025	0.009	−0.152	0.054	0.067
DOP	−0.076	0.001	−0.006	0.010	−0.129	0.086	0.215
$Si(OH)_4$	−1.535	0.070	0.275	−0.070	−3.044	1.316	2.807

[a]Positive value means northeastward. The unit of velocity flux (i.e., volume transport through a unit width) is $m^2\ s^{-1}$, and the unit of other quantities is $\mu M\ m^2\ s^{-1}$.

the combination of field data with a numerical model is also necessary.

[47] Recently, the contribution of coastal nutrients to the primary production of the entire ocean has been estimated by a global model [*Giraud et al.*, 2008]. Because of model resolution limitations, many coastal physical processes including the formation of a thermohaline front are not represented by the global model. A revised estimate is therefore necessary in the future, with a combination of a global model and a regional high resolution model that can represent the formation of thermohaline fronts and other coastal processes.

[48] **Acknowledgments.** This study was funded by NSFC and RGC (40218001, 40925017, and N-HKUST609/02) and by the Ministry of Science and Technology of P. R. China (2007DFB20380). Xinyu Guo acknowledges the support from JSPS KAKENHI (21310012). We thank Dr. Lei Wang for discussion; Bing Deng, J. C. Chen, H. Wei, L. X. Dong, and colleagues from the Ocean University of China for their help in field and laboratory experiments; and Qingji Li for his contribution to Figure 3. We thank the captain and crew of the R/V 'Yan Ping 2' for their assistance onboard. We also thank the Associate Editor and the four anonymous reviewers for their constructive comments on improving the original manuscript.

References

Akitomo, K., N. Imasato, and T. Awaji (1990), A numerical study of a shallow sea front generated by buoyancy flux: Generation mechanism, *J. Phys. Oceanogr.*, *20*, 172–189, doi:10.1175/1520-0485(1990)020<0172:ANSOAS>2.0.CO;2.

Brandini, F. P., D. Boltovskoy, A. Piola, S. Kocmur, R. Röttgers, P. C. Abreu, and R. M. Lopes (2000), Multiannual trends in fronts and distribution of nutrients and chlorophyll in the southwestern Atlantic (30–62°S), *Deep Sea Res., Part I*, *47*, 1015–1033, doi:10.1016/S0967-0637(99)00075-8.

Cai, W. J., M. Dai, Y. Wang, W. Zhai, T. Huang, S. Chen, F. Zhang, Z. Chen, and Z. Wang (2004), The biogeochemistry of inorganic carbon and nutrients in the Pearl River estuary and the adjacent northern South China Sea, *Cont. Shelf Res.*, *24*, 1301–1319, doi:10.1016/j.csr.2004.04.005.

Candela, J., R. C. Beardsley, and R. Limeburner (1992), Separation of tidal and subtidal currents in ship-mounted acoustic Doppler current profiler observations, *J. Geophys. Res.*, *97*, 769–788, doi:10.1029/91JC02569.

Carrillo, L., A. J. Souza, A. E. Hill, J. Brown, L. Fernand, and J. Candela (2005), Detiding ADCP data in a highly variable shelf sea: The Celtic Sea, *J. Atmos. Oceanic Technol.*, *22*, 84–97, doi:10.1175/JTECH-1687.1.

Chen, C. C., F. K. Shiah, S. W. Chung, and K. K. Liu (2006), Winter phytoplankton blooms in the shallow mixed layer of the South China Sea enhanced by upwelling, *J. Mar. Syst.*, *59*, 97–110, doi:10.1016/j.jmarsys.2005.09.002.

Chen, C. T. A. (2008), Distributions of nutrients in the East China Sea and the South China Sea connection, *J. Oceanogr.*, *64*, 737–751, doi:10.1007/s10872-008-0062-9.

Chen, C. T. A., S.-L. Wang, B.-J. Wang, and S.-C. Pai (2001), Nutrient budgets for the South China Sea basin, *Mar. Chem.*, *75*, 281–300, doi:10.1016/S0304-4203(01)00041-X.

Chu, P. C., and G. Wang (2003), Seasonal variability of thermohaline front in the central South China Sea, *J. Oceanogr.*, *59*, 65–78, doi:10.1023/A:1022868407012.

Endoh, M. (1977), Formation of thermohaline front by cooling of the sea surface and inflow of the fresh water, *J. Oceanogr. Soc. Jpn*, *33*, 6–15, doi:10.1007/BF02110843.

Foreman, M. G. G., and H. J. Freeland (1991), A comparison of techniques for tide removal from ship-mounted acoustic Doppler measurements along the southwest coast of Vancouver Island, *J. Geophys. Res.*, *96*, 17,007–17,021.

Giraud, X., C. Le Quéré, and L. C. da Cunha (2008), Importance of coastal nutrient supply for global ocean biogeochemistry, *Global Biogeochem. Cycles*, *22*, GB2025, doi:10.1029/2006GB002717.

Grasshoff, K., K. Kremling, and M. Ehrhardt (Eds.) (1999), *Methods of Seawater Analysis*, 3rd ed., Wiley, Weinheim, Germany, doi:10.1002/9783527613984.

Jakobsen, F. (1997), Hydrographic investigation of the Northern Kattegat front, *Cont. Shelf Res.*, *17*(5), 533–554, doi:10.1016/S0278-4343(96)00044-1.

Kachel, N. B., G. L. Hunt Jr., S. A. Salo, J. D. Schumacher, P. J. Stabeno, and T. E. Whitledge (2002), Characteristics and variability of the inner front of the southeastern Bering Sea, *Deep Sea Res., Part II*, *49*, 5889–5909, doi:10.1016/S0967-0645(02)00324-7.

Lee Chen, Y. L. (2005), Spatial and seasonal variations of nitrate-based new production and primary production in the South China Sea, *Deep Sea Res., Part I*, *52*, 319–340, doi:10.1016/j.dsr.2004.11.001.

Lee Chen, Y. L., and H. Y. Chen (2006), Seasonal dynamics of primary and new production in the northern South China Sea: The significance of river discharge and nutrient advection, *Deep Sea Res., Part I*, *53*, 971–986, doi:10.1016/j.dsr.2006.02.005.

Li, C., J. R. Nelson, and J. V. Koziana (2003), Cross-shelf passage of coastal water transport at the South Atlantic Bight observed with MODIS Ocean Color/SST, *Geophys. Res. Lett.*, *30*(5), 1257, doi:10.1029/2002GL016496.

Liu, K.-K., S.-Y. Chao, P.-T. Shaw, G.-C. Gong, C.-C. Chen, and T. Y. Tang (2002), Monsoon-forced chlorophyll distribution and primary production in the South China Sea: Observations and a numerical study, *Deep Sea Res., Part I*, *49*, 1387–1412, doi:10.1016/S0967-0637(02)00035-3.

Liu, S. M., J. Zhang, H. T. Chen, and G. S. Zhang (2005), Factors influencing nutrient dynamics in the eutrophic Jiaozhou Bay, North China, *Prog. Oceanogr.*, *66*, 66–85, doi:10.1016/j.pocean.2005.03.009.

Liu, S. M., G.-H. Hong, J. Zhang, X. W. Ye, and X. L. Jiang (2009), Nutrient budgets for large Chinese estuaries, *Biogeosciences*, *6*, 2245–2263, doi:10.5194/bg-6-2245-2009.

Naveira Garabato, A. C. N., V. H. Strass, and G. Kattner (2002), Fluxes of nutrients in a three-dimensional meander structure of the Antarctic Polar Front, *Deep Sea Res., Part II*, *49*, 3771–3792, doi:10.1016/S0967-0645(02)00110-8.

Ning, X., F. Chai, H. Xue, Y. Cai, C. Liu, and J. Shi (2004), Physical-biological oceanographic coupling influencing phytoplankton and primary production in the South China Sea, *J. Geophys. Res.*, *109*, C10005, doi:10.1029/2004JC002365.

Pan, L., J. Zhang, Q. Chen, and B. Deng (2005), Picoplankton community structure at a coastal front region in the northern part of the South China Sea, *J. Plankton Res.*, *28*(3), 337–343, doi:10.1093/plankt/fbi117.

Read, J. F., M. I. Lucas, S. E. Holley, and R. T. Pollard (2000), Phytoplankton, nutrients and hydrography in the frontal zone between the Southwest Indian Subtropical gyre and the Southern Ocean, *Deep Sea Res., Part I*, *47*, 2341–2368, doi:10.1016/S0967-0637(00)00021-2.

Song, X., L. Huang, J. Zhang, X. Huang, J. Zhang, J. Yin, Y. Tan, and S. Liu (2004), Variation of phytoplankton biomass and primary production in Daya Bay during spring and summer, *Mar. Pollut. Bull.*, *49*, 1036–1044, doi:10.1016/j.marpolbul.2004.07.008.

Su, J. L. (1998), Circulation dynamics of the China Seas: North of 18N, in *The Sea, The Global Coastal Ocean: Regional Studies and Syntheses*, vol. 11, edited by A. R. Robinson and K. Brink, pp. 483–506, Wiley, New York.

Wang, D., Y. Liu, Y. Qi, and P. Shi (2001), Seasonal variability of thermal fronts in the northern South China Sea from satellite data, *Geophys. Res. Lett.*, *28*(20), 3963–3966, doi:10.1029/2001GL013306.

Xu, J., K. Yin, L. He, X. Yuan, A. Y. T. Ho, and P. J. Harrison (2008), Phosphorus limitation in the northern South China Sea during late summer: Influence of the Pearl River, *Deep Sea Res., Part I*, *55*, 1330–1342, doi:10.1016/j.dsr.2008.05.007.

Yanagi, T. (1987), Classification of 'Siome', streaks and fronts, *J. Oceanogr. Soc. Jpn*, *43*, 149–158, doi:10.1007/BF02109215.

Yanagi, T., and T. Sanuki (1991), Variation in the thermohaline front at the Mouth of Tokyo Bay, *J. Oceanogr. Soc. Jpn*, *47*, 105–110, doi:10.1007/BF02301060.

Yanagi, T., X. Guo, T. Saino, T. Ishimaru, and S. Noriki (1997), Thermohaline front at the mouth of Ise Bay, *J. Oceanogr.*, *53*, 403–409.

Yin, K., and P. J. Harrison (2007), Influence of the Pearl River estuary and vertical mixing in Victoria Harbor on water quality in relation to eutrophication impacts in Hong Kong waters, *Mar. Pollut. Bull.*, *54*, 646–656, doi:10.1016/j.marpolbul.2007.03.001.

Yoshioka, H. (1971), Oceanic front at Kii-Suido in winter (1) (in Japanese), *Umi Sora*, *46*, 1–31.

Zhang, J., and J. L. Su (2006), Nutrient dynamics of the China Seas: The Bohai Sea, Yellow Sea, East China Sea and South China Sea, in *The Sea*, vol. 14, edited by A. R. Robinson and K. H. Brink, pp. 637–671, Wiley, New York.

Zhang, J., Z. G. Yu, J. T. Wang, J. L. Ren, H. T. Chen, H. Xiong, L. X. Dong, and W. Y. Xu (1999), The subtropical Zhujiang (Pearl River) Estuary:

Nutrient, trace species and their relationship to photosynthesis, *Estuarine Coastal Shelf Sci.*, *49*, 385–400, doi:10.1006/ecss.1999.0500.

Zhang, J., S. M. Liu, J. L. Ren, Y. Wu, and G. L. Zhang (2007), Nutrient gradients from the eutrophic Changjiang (Yangtze River) Estuary to the oligotrophic Kuroshio waters and re-evaluation of budgets for the East China Sea Shelf, *Prog. Oceanogr.*, *74*, 449–478, doi:10.1016/j.pocean.2007.04.019.

Y. F. Bi, J. B. Li, S. M. Liu, X. Luo, and J. Zhang, Key Laboratory of Marine Chemistry Theory and Technology, Ministry of Education, Ocean University of China, 238 Songling Road, Qingdao, 266100, China. (sumeiliu@ouc.edu.cn)

Q. Chen, Laboratory of Ocean Dynamic Processes and Satellite Oceanography, Second Institute of Oceanography, State Oceanic Administration, Xixihexia No. 9, Hangzhou 310012, China.

X. Guo, Center for Marine Environmental Studies, Ehime University, 2-5 Bunkyo-Cho, Matsuyama 790-8577, Japan.